ELSEVIER

Contents lists available at ScienceDirect

Electrochimica Acta

journal homepage: www.journals.elsevier.com/electrochimica-acta



Effects of ion mass transport on electrochemical reaction pathways in aluminum-anthraquinone batteries

Harrison Y. Asare ^{a,b}, Surabh S. KT ^c, Leo W. Gordon ^c, George John ^{a,b,*}, Robert J. Messinger ^{b,c,*}

- a Department of Chemistry and Biochemistry, Center for Discovery and Innovation, The City College of New York, CUNY, New York, New York 10031, United States
- b The Ph.D. Program in Chemistry, The Graduate Center of the City University of New York, New York, New York 10016, United States
- ^c Department of Chemical Engineering, The City College of New York, CUNY, New York, New York 10031, United States

ARTICLE INFO

Keywords: Aluminum batteries Organic batteries Anthraquinone Mass transport limitations Electrochemical reaction pathway Damkohler number

ABSTRACT

Aluminum anodes and quinone-based organic cathodes couple as earth abundant, sustainable, and safe battery electrodes. However, different numbers of galvanostatic discharge plateaus have been observed in aluminum-quinone cells depending on the experimental conditions, a phenomenon that has not yet been explained and furthermore affects cell energy density. Here, in aluminum-anthraquinone batteries, we show that ion mass transport affects the electrochemical reaction pathway and controls the occurrence of either one or two reduction plateaus during galvanostatic discharge. The effects of electrode mass loading, porosity, rest periods, and cycling rates were analyzed on the reduction potential and relative specific capacity of the galvanostatic plateaus. When $AlCl_2^+$ cations charge compensate the electrochemically reduced carbonyl groups concurrently, a single reduction plateau is observed. When ion mass transport is limiting, sequential reduction and charge compensation of each carbonyl group results in two distinct reduction plateaus. The second plateau occurs at a potential approximately 0.3 V lower than the first, thus decreasing the cell energy density. The potential of the electrochemical oxidation reaction where $AlCl_2^+$ cations dissociate, however, is not affected. Ion mass transport is thus shown to be a critical variable that can control the electrochemical reaction pathway, redox potentials, and practical energy densities of aluminum-quinone batteries.

1. Introduction

Aluminum (Al)-organic batteries couple Al metal anodes to organic materials to address flammability [1], sustainability [2], toxicity of cobalt, and humanitarian issues [3] associated with the lithium-ion batteries. Organic electrodes are sustainable, renewable, and tunable at a molecular level, and furthermore, have the unique ability to coordinate to different counterions [4,5]. This flexibility toward counterions makes it possible to build a range of battery technologies that are not based on scarce and unsafe metal anodes, but rather on using abundant and safe materials like aluminum [6]. Amongst metal anodes, aluminum metal is promising due to its high volumetric and gravimetric capacities, abundant availability, low cost, sustainability, and innate safety [7,8].

Researchers in Al-organic batteries have incorporated a diverse range of molecular structural designs that utilize redox-active groups from the array of functionalities available for organic molecules. Various organic structural motifs and functional groups used in Al-organic batteries include metal-organic frameworks that are hydrogen bonded to polyimide redox groups as demonstrated by Zhou et al.[9], bipolar-type covalent organic framework electrode reported by Liu et al. [10], polymer-based electrodes have also been reported [11,12], and molecular electrodes using amine [13,14] and carbonyl [12,15–20] redox groups. Quinones contain carbonyl redox groups and have been used as electrode materials in various metal-organic batteries because of their highly reversible keto-enol transformation during electrochemical redox [21]. The first instance of a keto-enol transformation in an Al-organic battery was reported in 2019, where Kim et al. [18] synthesized a phenanthrene quinone triangle to store three electrons per molecule followed by charge compensation with chloroaluminate (AlCl₂) cations.

Recent investigations have shed light on the ionic and electronic charge storage mechanisms of quinone-based electrodes in aluminum batteries. Using indanthrone quinone, Gordon et al. [16] coupled solid-state nuclear magnetic resonance (NMR) spectroscopy and

E-mail addresses: gjohn@ccny.cuny.edu (G. John), rmessinger@ccny.cuny.edu (R.J. Messinger).

^{*} Corresponding authors.

electrochemical methods to experimentally elucidate the charge storage mechanism at the molecular level, revealing that chloroaluminous AlCl₂ cations are the charge compensating ions. Soon after, Gordon et al. [17] elucidated that 1,5-dichloroanthraquinone complexed monovalent AlCl₂⁺ ions and delineated the effects of electrolyte ion speciation on the coordination environments of the counterions in different electrolytes using a combination of NMR spectroscopy and DFT calculations. Thus, chloroaluminous, AlCl₂ cations have been shown to charge compensate anthraquinone-based and other organic electrode materials after their electrochemical reduction [10,13-15,18]. Note that other reports have identified the divalent aluminum chloride cation (AlCl²⁺) as the charge compensating ion in other, non-quinone-based organic molecules. You et al. demonstrated the coordination of AlCl²⁺ to tetradiketone macrocycle by affirming the preferred binding energies of the tetradiketone-AlCl²⁺ complex using density functional theory (DFT) [20]. Critically, the active carbonyl groups in this study were not in a quinone-type configuration, resulting in a different mechanism for complexation than in quinone-based materials. Overall, technological development of Al-organic batteries has been hindered in part due to incomplete understanding of the electrochemical redox mechanisms.

9,10-anthraquinone (AQ) is a foundational quinone structure with two carbonyl groups on the central ring of an anthracene base and has previously been studied in Al-organic batteries [12,19,22]. On discharge, Al-AQ batteries operate via one-electron electrochemical reductions of each carbonyl group and ionic charge compensation by chloroaluminous AlCl₂⁺ cations. On charge, the AQ-counterion comelectrochemically oxidized, charge-compensating cations, and resulting in the AQ starting material [16]. Bitenc et al. [12] first studied Al-AQ batteries using an electrolyte consisting of aluminum chloride (AlCl₃) and 1-ethyl-3-imidazolium chloride [EMIm]Cl in a molar ratio of 1.5 at a rate of C/5, or 51.5 mA/g. Here, their galvanostatic cycling experiments yielded discharge plateaus at ca. 1.1 and 0.8 V with a specific capacity of 180 mAh/g. They proposed divalent chloroaluminous $AlCl^{2+}$ as the charge compensating cation. Later, Zhou et al. [19] showed that the galvanostatic cycling of the Al-AQ battery yielded only one plateau by the second cycle at 20 mA/g, achieving 215 mAh/g, close to the theoretical specific capacity of two electrons per AQ molecule (257 mAh/g). Zhou et al. [19] claimed that Al³⁺ ion is the counterion that charge compensated the reduced AQ. Aside from the reports from Bitenc et al. [12] and Zhou et al. [19] on Al-AQ, Kao et al. [22] also showed the existence of two plateaus in an Al-AQ battery at 160 mAh/g while comparing the influence of molecular structure on redox voltages and specific capacity on cycle one of different quinone-based molecules. Despite using modestly different cycling rates and similar composite electrode compositions and voltage cut-off windows, both Bitenc et al. [12] and Zhou et al. [19] interestingly observed two and one galvanostatic reduction plateaus (Table S1), respectively.

To date, no Al-organic battery reports explain the occurrence of different numbers of galvanostatic reduction reactions. Other reports investigating the electrochemical behavior of the AQ in protic-solvent-based electrolytes suggest the co-insertion of hydrogen and the counterion in the electrolytes [23,24] afforded the two discharge plateaus. Another report also suggested that supporting ions can associate with the reduced AQ to yield multiple ions charge compensating reduction reactions to afford two discharge plateaus [25]. Understanding the origin of the different number of galvanostatic discharge plateaus observed in Al-AQ batteries will aid the rational design of Al-organic batteries.

Here, we explain the yet unknown basis of the lower-potential discharge reaction in Al-AQ batteries and provide experimental evidence to demonstrate the variables controlling one or two plateaus in Al-AQ batteries. Ion mass transport is shown to be the crucial phenomenon controlling the number of discharge plateaus after testing the effects of different cell design methods and cycling conditions. We tailored the electrode design and cycling conditions to control ion mass transport

limitations by using different composite electrode mass loadings, porosities, electrode wetting times, and cycling rates. Density functional theory (DFT) calculations show that concurrent and sequential redox pathways are both thermodynamically feasible, consistent with the presence of either one or two electrochemical plateaus depending on the mass transport or reaction limitation conditions.

2. Materials and methods

2.1. Electrode preparation

Composite electrodes were fabricated by ball milling anthraquinone (65 wt. %; ThermoFisher, > 98%) and conductive carbon (25 wt. % super P; Alfa Aesar, 99 %) into a fine mixture in a stainless-steel vessel for 1 h. A 10 wt. % solution of polyvinylidene fluoride (average molecular weight of 534,000 g/mol; Sigma-Aldrich) dissolved in N-methyl2-pyrrolidone (NMP) was used as the binder. An electrode slurry was formed by spinning at 2000 rpm for 10 min using a Thinky Corporation ARE-310 planetary mixer and casted using a doctor blade onto a molybdenum foil (0.025-mm thick; Alfa Aesar, 99.95 %) as the current collector. The composite electrode was dried in a fume hood until it appeared dry and then transferred into a vacuum oven at 100° C for 24 h to evaporate residual NMP. The mass loading was varied between 0.24 mg/cm² to 4.89 mg/cm².

2.2. Cell Fabrication

All cells were constructed in an argon-filled glovebox (VAC, <1 ppm O_2 and H_2O). A Lewis acidic mixture of aluminum chloride (AlCl $_3$) (Alfa Aesar, 99.99 % metal basis) and 1-ethyl-3-methylimidazolium chloride ([EMIm]Cl) (Aldrich, \geq 98.0 %) was prepared in a 1.5:1 molar ratio of AlCl $_3$:[EMIm]Cl and used as the electrolyte. Poly(tetrafluoroethylene) (PTFE) Swagelok-type unions with 12.7-mm diameters were used as airtight cells bodies and cylindrical molybdenum rods were used as current collectors. Al foil (0.1-mm thick; Alfa Aesar, 99.99 %) and composite AQ electrodes were punched into 12-mm diameter circular disks and used as anodes and cathodes, respectively. Glass microfiber filters (Whatman, GF/D) were punched into 13-mm diameter circular disks and used as separators.65 μ L of the electrolyte was added to each cell.

2.3. Electrochemical measurements

All galvanostatic experiments were performed at room temperature on an Arbin Instruments LBT battery cycler at 25°C . Fabricated cells were rested for 1 h or 24 h and cycled at a constant current of either 10,50, or $250\,\text{mA/g}$ within $0.30\,\text{V}$ and $1.9\,\text{V}$ for the lower and upper voltage limits respectively. Cells underwent a consecutive $10\,$ min rest in between the charge and discharge cycles. The cycles were repeated for at least $10\,$ cycles to observe trends in the number of first and second plateaus. Variable-rate cyclic voltammetry (CV) experiments were performed on a six-channel BioLogic VSP-300 potentiostat using various scan rates from 0.10 to $10\,$ mV/s between $0.30\,$ – $1.9\,$ V. Five cycles were conducted for each scan rate with an initial rest of $1\,$ h at room temperature.

2.4. Density functional theory calculation

All DFT calculations were conducted using Gaussian 16 with the 6-31G+(d,p) basis set with the Becke-Lee-Yang-Parr (B3LYP) hybrid exchange-correlation functional. Initially, the molecular structures of AQ and $AlCl_2^+$ cations were constructed in GaussView 06 and geometrically optimized. Various AQ-AlCl $_2^+$ complexes were optimized by placing the $AlCl_2^+$ cation at approximately 3.0 Å from the carbonyl oxygens of AQ. Once the geometry was optimized, frequency calculations were performed using the same level of theory. Gibb's free energies and

enthalpies of different complexes were calculated by computing the differences between the products and reactants.

2.5. NMR spectroscopy

Liquid-state 1 H single-pulse nuclear magnetic resonance (NMR) experiments were performed on a 7.05 T Bruker Avance III HD spectrometer equipped with BBFO probe operating at 300.13 MHz. Samples were acquired in a 5-mm diameter glass tube with an inserted 3-mm diameter glass tube containing D_2O (Sigma-Aldrich, ≥ 99.85 %) for locking and as a 1 H chemical shift reference at 4.70 ppm.

3. Results and discussion

Our interest in understanding the origin of one or two reduction plateaus stems from the inconsistency of these reactions reported in existing Al-AQ literature [12,19]. When the Al-AQ cell is discharged, the presence of a second reduction reaction at a lower potential (approximately 0.80 V) affords lower energy compared to an equivalent cell that produces a single discharge plateau at ca. 1.1 V. We hypothesize that the occurrence of either one or two reduction plateaus stems from different electrochemical reaction pathways. Specifically, we propose that the AO carbonyl groups can be reduced either sequentially or concurrently, manifesting as two one-electron reactions at distinct potentials and one 'two-electron' reaction at the same potential, respectively. The sequential reaction occurs under mass-transport limited conditions, where the radical anionic (semiquinone) form cannot be effectively charge compensated before being further reduced. In contrast, the concurrent mechanism will occur in situations where the semiquinone form is immediately charge compensated. These reaction mechanisms are the expected galvanostatic cycling profiles corresponding to each mechanism are shown in Fig. 1. Building on previous work, we expand the understanding of the two-electron reduction coupled with compensation by two AlCl₂⁺ cations by detailing the differences between

mass-transport limited conditions and reaction-limited conditions, showing that the availability of complexing ions ultimately affects the electrochemical reduction potentials.

Using the electrochemical framework of Schoetz et al. [26], the interplay between mass transport and electrochemical kinetics can be quantified by the electrochemical Damköhler number, Da_{el} , which is the dimensionless ratio of the apparent rate of the electrochemical reaction, r_{rxn}^{app} , including any surface processes, to the rate of mass transport of ions to the surface, r_m .

$$Da_{el} = \frac{r_{rxn}^{app}}{r_{r}} \tag{1}$$

The apparent rate of the electrochemical reaction is

$$r_{rxn}^{app} = \frac{j_{rxn}^{app}}{z_{r}F} \tag{2}$$

where $j_{r,m}^{app}$ is the current density due to the electrochemical reaction, including any surface processes, z_e is the number of electrons transferred per reaction species or ion, and F is Faraday's constant. For electrochemical reactions that follow Butler-Volmer kinetics, the current $(j_{r,m}^{app})$ associated with the reaction is

$$j_{rxn}^{app} = j_o \left[exp \left(\frac{\alpha_a F}{RT} \eta_s \right) - exp \left(\frac{\alpha_c F}{RT} \eta_s \right) \right]$$
 (3)

where R is the gas constant, T is the temperature, j_o is the exchange current density, α_a and α_c are the anodic and cathodic transfer coefficients respectively, and η_s is the charge transfer overpotential. The rate of mass transport $r_{\rm m}$ is simply equal to the mass flux N, as defined by the Nernst-Planck equation:

$$N = -D\nabla c - \frac{zF}{RT}Dc\nabla\varphi \tag{4}$$

The first term describes the diffusion of ions across a concentration

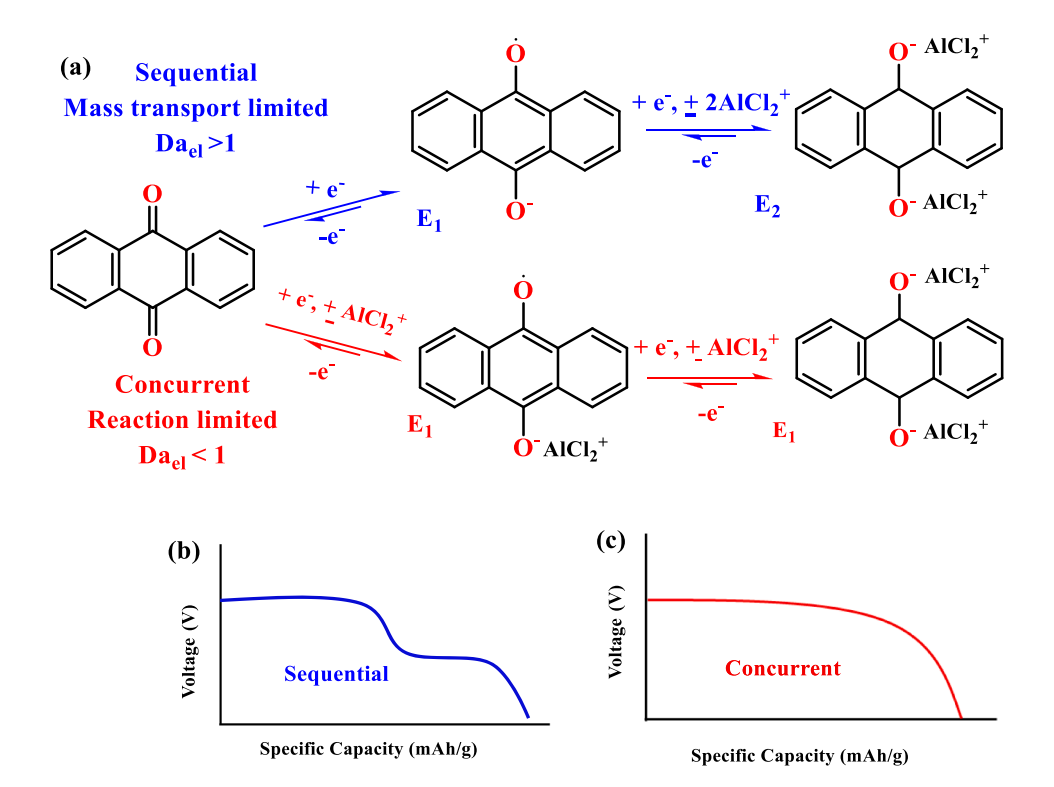


Fig. 1. (a) Schematic of the sequential (blue) and concurrent (red) electrochemical pathways that can occur during the electrochemical cycling of anthraquinone electrodes. Chloroaluminous $AlCl_2^+$ cations charge compensates the reduced carbonyl functional groups. (b) Under mass-transport-limited conditions ($Da_{el} > 1$), sequential electrochemical reduction of the carbonyl groups occurs at two distinct potentials, while (c) concurrent reduction occurs under reaction-limited conditions ($Da_{el} < 1$) at a single potential.

gradient (∇c) with a diffusion constant (D). The second term is migration, and it involves the flux of ions due to the force of an electric field ($\nabla \varphi$) for a set number of electrons transported (z). Furthermore, if the electromigrative flux is small compared to the diffusive flux, then the rate of mass transfer is simply the diffusive flux, or $r_m \approx -D\nabla c$.

The sequential reaction pathway will occur when the overall electrochemical reaction is mass-transport-limited (Da $_{\rm el}>1$). This sequential pathway would result in the second AlCl $_{\rm 2}^{\rm 2}$ molecule complexing at a lower potential compared to the first AlCl $_{\rm 2}^{\rm 2}$ molecule.

When the sequential pathway is broken into a microkinetic model, i. e., a sequence of binary molecular events, the quinones would first form the semiquinone radical anion species, before being reduced to the dianion form, followed then by charge compensation [16,27,28]:

$$AQ + e^{-\frac{E_1}{2}}AQ^{-} \tag{5}$$

$$AQ^{-} + e^{-} \stackrel{E_2}{\to} AQ^{2-}$$
 (6)

$$AQ^{2-} + 2AlCl_2^+ \rightarrow AQ \cdot 2AlCl_2 \tag{7}$$

Note that the electrochemical reduction reactions (5) and (6) occur at different potentials, E_1 and E_2 , respectively.

The concurrent reaction pathway will occur when the overall electrochemical process is reaction-limited (Da $_{\rm el}$ < 1). The microkinetic model for the concurrent pathway would also involve generation of the radical semiquinone species, however, charge compensation would occur after each reduction step:

$$AQ + e^{-\frac{E_1}{2}}AQ^{-} \tag{8}$$

$$AQ^{-} + AlCl_2^{+} \rightarrow AQ \cdot AlCl_2 \tag{9}$$

$$AQ \cdot AlCl_2 + e^{-\frac{E_1}{2}} AQ^{-} \cdot AlCl_2$$
 (10)

$$AQ^{-} \cdot AlCl_{2} + AlCl_{2}^{+} \rightarrow AQ \cdot 2AlCl_{2}$$

$$\tag{11}$$

Experimental evidence below indicates that the electrochemical reduction reactions (8) and (10) occur at the same potentials, E_1 .

The overall AQ reaction is shown in Equation 12

$$AQ + 4 Al_2Cl_7^- + 2e^- \Rightarrow AQ \cdot 2AlCl_2^+ + 6AlCl_4^-$$
 (12)

Interestingly, Voskian and Hatton [27] recently reported a solid-state faradaic electro-swing system for CO_2 capture, wherein CO_2 complexes with electrochemically reduced AQ reversibly to form carbonate moieties. An analogous mechanism was observed where a second reduction reaction was measured at a lower potential under mass-transport limitations (sequential reactions), relative to the equivalent experiment carried out under high CO_2 flux (concurrent reactions) [27,28]. The proposed reaction pathways are also plausible considering the two-electron reaction mechanism in n-type organic systems, where the redox active group is reduced to a radical anion and then subsequently reduced to a dianion [28].

3.1. Thermodynamic calculations

To inspect the thermodynamic feasibility of sequential and concurrent charge storage mechanisms, DFT calculations were performed to compute the electronic structures and thermodynamic properties of reduced anthraquinone molecules when coordinated to $AlCl_2^+$ cations in different configurations. Electrostatic potential maps were generated for (i) two AQ molecules, where one carbonyl group on one AQ molecule has been reduced, and one charge-compensating $AlCl_2^+$ cation between them $(AQ^- \cdot AlCl_2^+ \cdot AQ)$ complex, Fig. 2a), and (ii) two AQ molecules, where two carbonyl groups have been reduced on one AQ molecule, and two charge-compensating $AlCl_2^+$ cations between them $(AQ^2 \cdot 2AlCl_2^+ \cdot AQ)$ complex, Fig. 2b). The reaction energies and

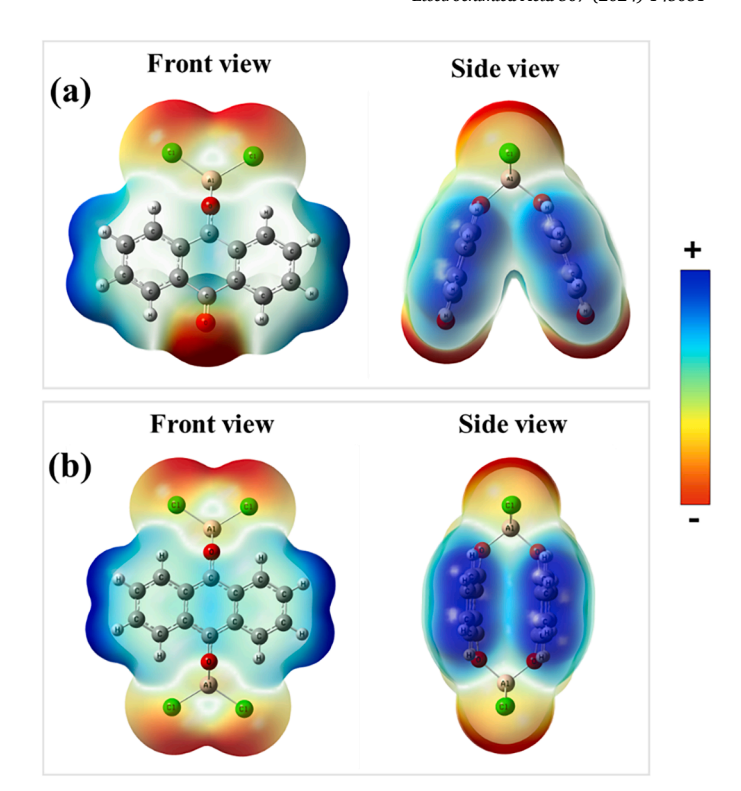


Fig. 2. Electrostatic potential maps of the different complexes. (a) Front and side view of an $AQ^{-}\cdot AlCl_2^+\cdot AQ$ complex. (b) Front view and side view of an $AQ^{2-}\cdot 2AlCl_2^+\cdot AQ$ complex.

enthalpies of formation of the complexes were calculated and tabulated (Table 1).

When complexes with two AQ molecules are considered (Fig. 2a and b), the DFT-optimized structures demonstrate that AlCl₂⁺ cations bind with aluminum in a tetrahedral geometry between the reduced enol and a carbonyl of the neutral AQ in its proximity. This tetrahedral aluminum coordination environment is consistent with that observed in other quinone-based molecules in Al batteries, as measured by solid-state ²⁷Al NMR spectroscopy [16,17]. The optimized structures shown are simplifications of the layered, periodic structure of AQ, that can accept a two-electron reduction per AO molecule [12,19].

The enthalpy and Gibb's free energy to form each complex were calculated (Table 1) to compare the energies of the complexed states. The calculations provide insights into the singly compensated state that supports the concurrent pathway (Fig. 2a) and the doubly compensated state that supports the sequential reduction reaction pathway (Fig. 2b). The DFT calculations indicated that the formation of all complexes are thermodynamically favorable due to their negative Gibb's free energies. The lowest Gibb's free energy was calculated when two AlCl½ cations coordinated with two AQ molecules (Fig. 2b, -426.06 kJ/mol), indicating that this is the moret thermodynamically favorable structure. In contrast, the Gibbs free energy of one AlCl½ cation coordinated to two AQ molecules was higher (Fig. 2a, -265.09 kJ/mol). Because the formation of both complexes studied are thermodynamically feasible, it

Table 1Enthalpies and Gibbs free energies corresponding to the formation of the complexes listed in Fig. 2, determined from their DFT-optimized structures.

Reaction	ΔH_{rxn} (kJ/mol)	ΔG_{rxn} (kJ/mol)
$\begin{aligned} 2AQ + 2Al_2Cl_7^- + & e^- \rightleftharpoons AQ \cdot AlCl_2^+ \cdot AQ + 3AlCl_4^- \\ AQ \cdot AlCl_2^+ \cdot AQ + 2Al_2Cl_7^- + & e^- \rightleftharpoons AQ^- \cdot 2AlCl_2^+ \cdot \\ AQ + 3AlCl_4^- \end{aligned}$	-230.07 -413.59	-265.09 -426.06

follows that ion mass transfer could indeed influence the electrochemical reaction pathway, as described in the microkinetic model in Equations 5-7 and 8-11.

3.2. Effects of mass loading

We first tested how ion mass transport affected the presence and evolution of the galvanostatic reduction plateaus by varying the electrode mass loading. A higher mass loading was expected to impede ion transport, resulting in greater mass-transport limitations that we hypothesized would favor sequential charge compensation (Da_{el} >1) of the reduced AQ at different redox potentials. A lower electrode mass loading, on the other hand, would reduce mass transport limitations and promote the concurrent reduction mechanism (Da $_{el}$ <1). A comparison between a higher mass loading of 4.89 mg/cm² and a lower mass loading of 0.24 mg/cm² (Fig. 3a) supported our hypothesis, showing that a lower mass loading (0.24 mg/cm²) produced evidence of two discharge plateaus in the first cycle, followed by one discharge plateau in subsequent cycles. However, the cell with a higher loading (4.89 mg/ cm²) demonstrates a greater extent of the lower-potential discharge reaction, even after the first ten cycles (Fig. 3b and c). Galvanostatic cycling data showing specific capacity vs. cycle number for these cells are presented in Figure S1. The results affirm that the sequential reaction mechanism occurred in the electrode with a higher mass loading, which has greater mass transport limitation. The results from the cell with lower electrode mass loading (0.24 mg/cm²) agreed with the hypothesized concurrent reduction mechanism arising from the abated mass transport limitation (Da_{el} <1).

The cell with a lower mass loading electrode showed an initial specific capacity of 240 mA h/g, close to the theoretical capacity of two-electron storage for a single AQ molecule. However, the tenth cycle produced a specific capacity of 120 mA h/g. The cell with a higher mass loading electrode showed a lower initial specific capacity of 60 mA h/g with lower specific capacities on subsequent cycles. We infer that the mass transport limitations in the cells are due to differences in mass loading influence the specific capacity and electrochemical reaction pathways.

3.3. Electrode compression experiments

Electrode compression experiments investigated the effects of porosity on mass transport and reaction limitations. Two composite electrodes with similar mass loadings (2.10–2.40 $\,$ mg/cm²) were selected. One of these electrodes was compressed using a hydraulic press under 20,000 psi to reduce the porosity from 60 % to 36 % (for calculation of electrode porosity, see Text S1, Supporting Information). The reduction in the porosity of the electrode should impede ion diffusion through the bulk electrode, resulting in an ionic mass transport limitation and driving the reaction mechanism towards sequential charge

compensation (Da_{el} >1). Galvanostatic cycling (Fig. 4a) demonstrated that both cells have two discharge plateaus that persist through at least 10 cycles. However, the second plateau is prominent in the cell with compressed composite electrodes on the tenth cycle due to the reduced porosity. Electrode compression introduces ionic mass transport limitations, therefore promoting the sequential reaction pathway. The galvanostatic cycling profiles of both cells demonstrated only one plateau after cycle 10 (Fig. 4b and c); however, the cell containing the compressed electrode exhibited lower specific capacities and greater polarization. Galvanostatic cycling data showing specific capacity vs. cycle number for these cells are presented in Figure S2. The low specific capacities are attributed to the inaccessible redox sites in the bulk electrode, suggesting that the reduced porosity impeded not only the rate of ion transport but also afforded sequential ion coordination.

3.4. Prolonged wetting time

The effects of electrode wettability were tested by resting two similarly fabricated cells for either 1 h or 24 h. To ensure the AQ was stable in the electrolyte for a prolonged duration, a mixture of AQ and the ionic liquid electrolyte was prepared and rested for 5 days. The liquid-state ¹H single-pulse NMR spectrum showed no new signals compared to the pristine electrolyte, indicating that AQ was insoluble in the electrolyte (Figure S3). The galvanostatic cycling data (Fig. 5a) demonstrates that allowing cells to rest improves electrolyte penetration into the bulk electrode, minimizing mass transport limitations. This finding is consistent with the report from Bitenc et al. [12] The discharge profiles of the cell rested for 24 h (Fig. 5a, black) demonstrate the prevalence of the higher-potential reaction in cycle 1 compared to the cell that rested only 1 h. This observation implies that reaction-limited charge compensation (Dael <1) occurs when electrodes are sufficiently wetted, resulting in the concurrent reaction pathway. By cycle 10 (approximately 20 h of cycling time), both cells demonstrated no visible plateau at a lower potential (Fig. 5b and c). Galvanostatic cycling data showing specific capacity vs. cycle number for these cells are presented in Figure S4. These results confirmed insufficient wetting results in ionic mass transport limitations and the sequential reaction pathway (Dael >1).

3.5. Effects of galvanostatic cycling rate

Three cells with similar mass loadings were subjected to galvanostatic cycling at rates of 10, 50, and 250 mA/g to study the effects of cycling rate on the reaction pathway (Fig. 6). Additional galvanostatic cycling data for these cells are shown in Figure S5. At the slowest rate of 10 mA/g, the first cycle yielded a predominantly single discharge plateau with a small capacity contribution from the second plateau (Fig. 6, blue solid line). The second plateau was completely absent in subsequent cycles. Here, the results demonstrate that under low current

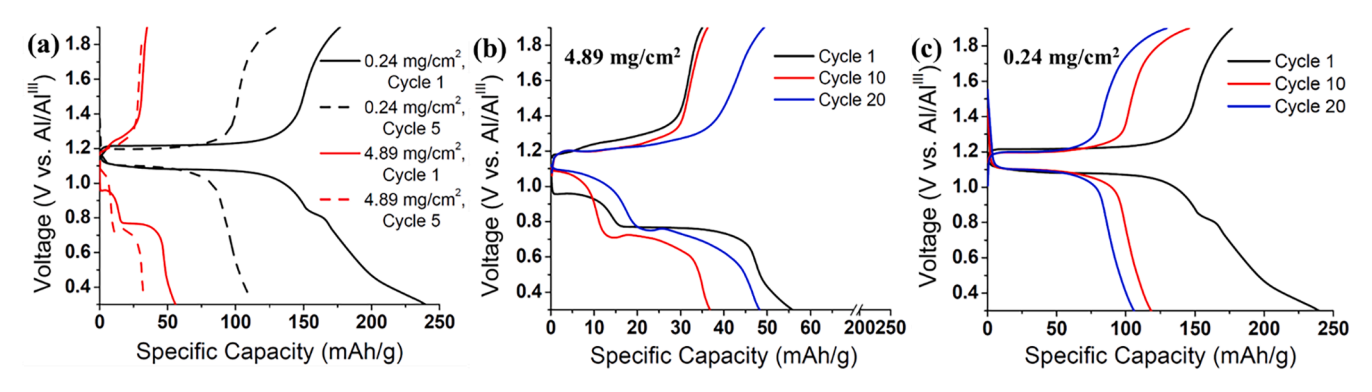


Fig. 3. Galvanostatic cycling performed at 50 mA/g on Al-AQ cells rested for 1 h with (a) a higher mass loading (4.89 mg/cm²) or a lower mass loading (0.24 mg/cm²) (cycles 1, 5). Additional cycles for the cell with a (b) higher mass loading or (c) lower mass loading.

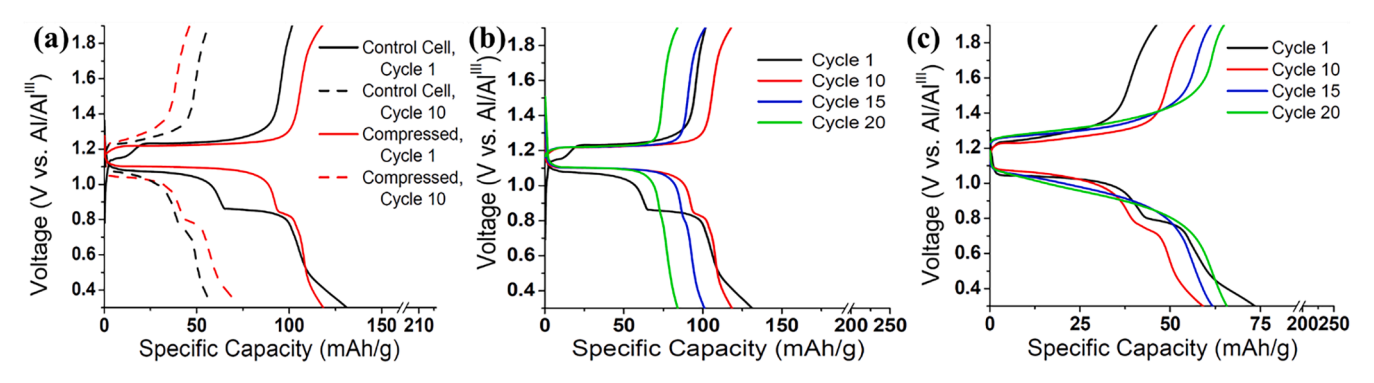


Fig. 4. Galvanostatic cycling performed at 50 mA/g on Al-AQ cells rested for 1 h with a (a) control electrode (2.37 mg/cm², 60 % porosity, black) or a compressed electrode (2.10 mg/cm², 36 % porosity, red) (cycles 1, 5). Additional cycles for the cell with a (b) control electrode or (c) compressed electrode.

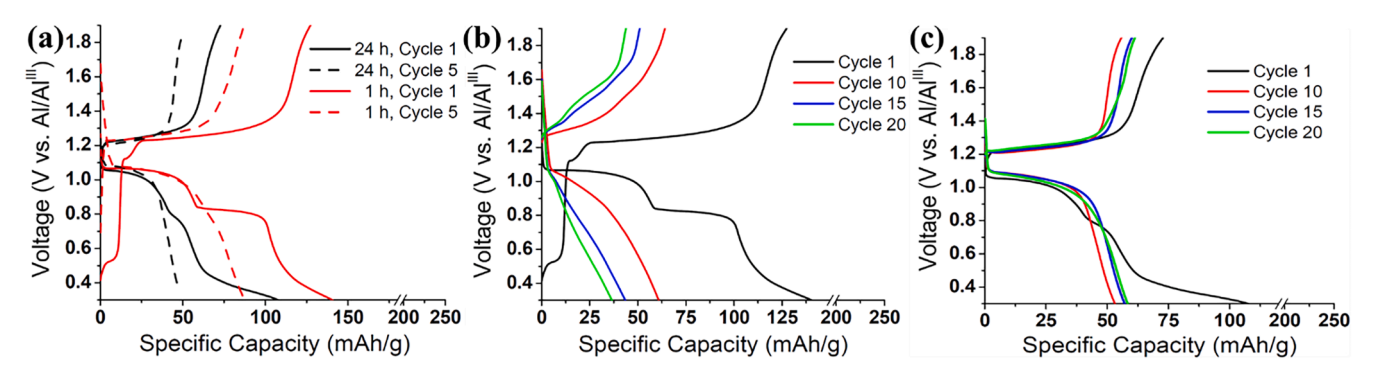


Fig. 5. Galvanostatic cycling performed at 50 mA/g on Al-AQ cells (a) rested for 24 h (2.31 mg/cm²) or 1 h (2.15 mg/cm²) before cycling (cycles 1,5). Additional cycles for the cell (b) rested 1 h or (c) 24 h.

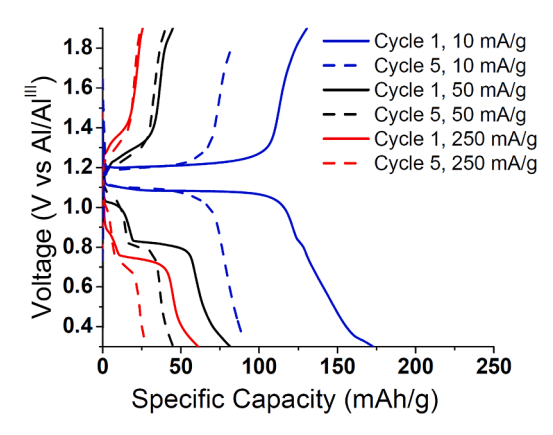


Fig. 6. Galvanostatic cycling of Al-AQ cells performed at 10 mA/g (blue, 2.44 mg/cm²), 50 mA/g (black, 2.35 mg/cm²) or 250 mA/g (red, 2.35 mg/cm²).

density, charge compensation is reaction-limited, hence a concurrent reaction (Da $_{\rm el}$ < 1).

Cells with higher current densities of 50 and 250 mA/g demonstrated a persisting plateau at the lower potential of 0.80 V, signifying that the sequential reaction pathway (Dael >1) was occurring. Interestingly, as the scan rate increased, there was only a minor capacity contribution from the reduction that occurred at the higher potentials (Fig. 6, red and black lines). The results suggest that under higher current densities, the reduction reactions occur at higher overpotentials where most of the carbonyls are reduced at the lower potential. The observations from the varied galvanostatic cycling rates are intuitive because, at low current densities, r_{xxn}^{app} is decreased, thereby decreasing Dael. Once Dael is sufficiently small, ions have sufficient time to diffuse to active sites in the electrode resulting in the concurrent charge compensation pathway.

Conversely, at high current densities, r_{rxp}^{app} is increased relative to r_m , thereby increasing Da_{el} . Hence, the cells cycled at higher current densities demonstrate increased polarization. The galvanostatic cycling experiments at different rates further suggest that the origin of the different reaction pathways can be an interplay between how electrochemical kinetics affect mass transport.

A table that details the experimental conditions and the number of reduction plateaus observed is shown in the Supporting Information (Table S1), which summarizes the results of this work as well as those observed in prior literature.

3.6. Variable-rate cyclic voltammetry

Variable-rate CV was performed to analyze the electrochemical reaction peaks of AQ in aluminum batteries under varying scan rates (Fig. 7). At slower scan rates (0.1 and 0.5 mV/s), there are two reduction peaks observed at approximately 1.0 V and overlapping peaks centered at 0.7 V, as well as two overlapping oxidative peaks centered near 1.35 V. Notably, two distinct oxidative events were not observed galvanostatically, and only appear to occur only at the slowest CV rates. The reductive and oxidative peaks broadened and merged as the scan rate increased (1.0 mV/s and above). This result shows that anthraquinone can undergo two reversible reactions during reduction and subsequent oxidation through a keto-enol transformation, in line with the discussed reduction mechanisms.

4. Conclusion

This work investigates the fundamental variables that dictate the electrochemical reaction pathways in Al-AQ batteries. We reveal that the ratio of the rates of ion mass transport to electrochemical kinetics are critical to the reaction pathway: under mass-transport-limited conditions (Da $_{\rm el}$ >1), the quinone carbonyl groups are electrochemically

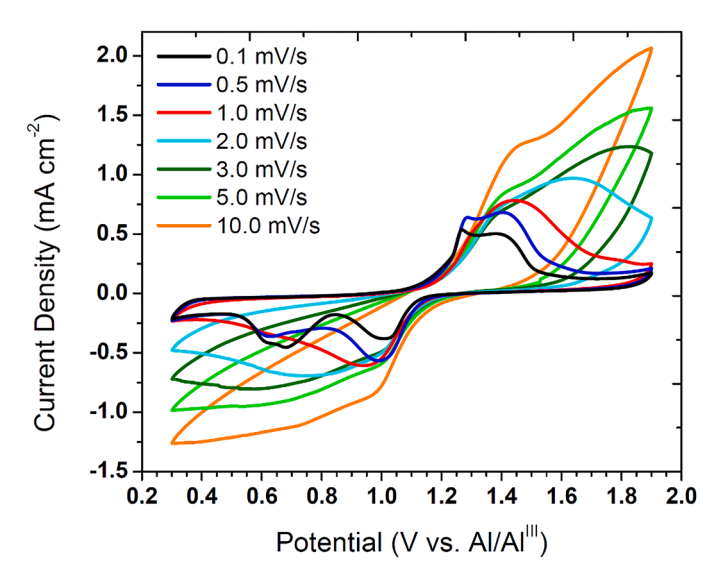


Fig. 7. Cyclic voltammogram of an Al-AQ cell conducted with scan rates of 0.1, 0.5, 1.0, 2.0, 3.0, 5.0, 10.0 mV/s.

reduced sequentially before being charge compensated, resulting in two distinct discharge potentials; in contrast, under reaction-limited conditions (Da $_{\rm el}$ <1), each carbonyl group is charge compensated as soon as it is reduced, resulting in equivalent discharge potentials for the two carbonyl groups. We showed that greater electrode mass loading, insufficient electrode wetting times, and higher current densities create mass-transport limitations sufficient to change the reaction pathway, whereas smaller electrode mass loading, ample wetting times, and lower current densities resulted in reaction-limited conditions and a single reduction potential. Critically, the electrochemical reduction reaction stemming from ion mass transport limited conditions occurs at a lower potential, decreasing cell energy density.

DFT calculations confirm the thermodynamic feasibility of both reaction pathways by demonstrating the stability of the doubly compensated state and the singly complexed state for thesequential and concurrent reduction pathways, respectively. Furthermore, chloroaluminous AlCl½ cations form tetrahedral aluminum coordination environments upon charge compensation, where the most energetically favorable configurations involve complexation of two AlCl½ cations with two AQ molecules. Overall, ion mass transport is shown to control the electrochemical reaction pathway, reduction potentials, and practical energy densities of aluminum-quinone batteries. Composite electrodes and electrochemical cycling parameters should be designed to reduce mass transfer limitations while balancing cell energy and power density requirements.

CRediT authorship contribution statement

Harrison Y. Asare: Writing – review & editing, Writing – original draft, Visualization, Methodology, Investigation, Formal analysis, Data curation, Conceptualization. Surabh S. KT: Methodology, Data curation. Leo W. Gordon: Writing – review & editing, Methodology, Investigation, Formal analysis, Conceptualization. George John: Supervision, Resources, Conceptualization. Robert J. Messinger: Writing – review & editing, Writing – original draft, Supervision, Methodology, Funding acquisition, Data curation, Conceptualization.

Declaration of competing interest

The authors declare that they have no known competing financial interests or personal relationships that could have appeared to influence the work reported in this paper.

Data availability

Data will be made available on request.

Acknowledgements

The authors gratefully acknowledge the U.S. National Aeronautics and Space Administration (NASA) for support via the NASA-CCNY Center for Advanced Batteries for Space under cooperative agreement 80NSSC19M0199. L.W.G. and R.J.M. additionally thank the U.S. National Science Foundation (NSF) for funding under NSF CAREER award CBET-1847552.

Supplementary materials

Supplementary material associated with this article can be found, in the online version, at doi:10.1016/j.electacta.2024.145031.

References

- K. Xu, Nonaqueous liquid electrolytes for lithium-based rechargeable batteries, Chem. Rev. 104 (2004) 4303–4418, https://doi.org/10.1021/cr030203g.
- [2] H. Chen, T.N. Cong, W. Yang, C. Tan, Y. Li, Y. Ding, Progress in electrical energy storage system: a critical review, Prog. Nat. Sci. 19 (2009) 291–312, https://doi. org/10.1016/j.pnsc.2008.07.014.
- [3] L. Leyssens, B. Vinck, C. Van Der Straeten, F. Wuyts, L. Maes, Cobalt toxicity in humans—a review of the potential sources and systemic health effects, Toxicology 387 (2017) 43–56, https://doi.org/10.1016/j.tox.2017.05.015.
- [4] M. Miroshnikov, K. Kato, G. Babu, N.K. Thangavel, K. Mahankali, E. Hohenstein, H. Wang, S. Satapathy, K.P. Divya, H. Asare, P.M. Ajayan, L.M.R. Arava, G. John, Made from henna! a fast-charging, high-capacity, and recyclable tetrakislawsone cathode material for lithium ion batteries, ACS Sustain. Chem. Eng. 7 (2019) 13836–13844, https://doi.org/10.1021/acssuschemeng.9b01800.
- [5] M. Miroshnikov, K. Kato, G. Babu, N. Kumar, K. Mahankali, E. Hohenstein, H. Wang, S. Satapathy, K.P. Divya, H. Asare, L.M.R. Arava, P.M. Ajayan, G. John, Nature-derived sodium-ion battery: mechanistic insights into Na-ion coordination within sustainable molecular cathode materials, ACS Appl. Energy Mater. 2 (2019) 8596–8604, https://doi.org/10.1021/acsaem.9b01526.
- [6] Recycling Rates of Metals, (n.d.). https://wedocs.unep.org/bitstream/handle/20. 500.11822/8702/Recycling_Metals.pdf?sequence=1&isAllowed=y (accessed November 29, 2021).
- [7] Y. Liu, W. Luo, S. Lu, Z. Zhang, Z. Chao, J. Fan, Novel carbonyl cathode for green and sustainable aluminum organic batteries, ACS Appl. Mater. Interfaces 14 (2022) 53702–53710, https://doi.org/10.1021/acsami.2c14365.
- [8] J. Chen, Q. Zhu, L. Jiang, R. Liu, Y. Yang, M. Tang, J. Wang, H. Wang, L. Guo, Rechargeable aqueous aluminum organic batteries, Angew. Chem. 133 (2021) 5858–5863, https://doi.org/10.1002/ange.202011144.
- [9] J. Zhou, X. Yu, J. Zhou, B. Lu, Polyimide/metal-organic framework hybrid for high performance Al - organic battery, Energy Storage Mater 31 (2020) 58–63, https:// doi.org/10.1016/j.ensm.2020.05.029.
- [10] Y. Liu, Y. Lu, A. Hossain Khan, G. Wang, Y. Wang, A. Morag, Z. Wang, G. Chen, S. Huang, N. Chandrasekhar, D. Sabaghi, D. Li, P. Zhang, D. Ma, E. Brunner, M. Yu, X. Feng, Redox-bipolar polyimide two-dimensional covalent organic framework cathodes for durable aluminium batteries, Angew. Chem. Int. Ed. 62 (2023) e202306091, https://doi.org/10.1002/anie.202306091.
- [11] N. Lindahl, J. Bitenc, R. Dominko, P. Johansson, Aluminum metal-organic batteries with integrated 3D thin film anodes, Adv. Funct. Mater. 30 (2020) 2004573, https://doi.org/10.1002/adfm.202004573.
- [12] J. Bitenc, N. Lindahl, A. Vizintin, M.E. Abdelhamid, R. Dominko, P. Johansson, Concept and electrochemical mechanism of an Al metal anode – organic cathode battery, Energy Storage Mater 24 (2020) 379–383, https://doi.org/10.1016/j. ensm.2019.07.033.
- [13] R. Grieco, O. Luzanin, D. Alvan, M. Liras, R. Dominko, N. Patil, J. Bitenc, R. Marcilla, A phenazine-based conjugated microporous polymer as a high performing cathode for aluminium-organic batteries, Faraday Discuss 250 (2024) 110-128. https://doi.org/10.1039/D3FD00132F.
- [14] S. Wang, S. Huang, M. Yao, Y. Zhang, Z. Niu, Engineering active sites of polyaniline for AlCl₂ + storage in an aluminum-ion battery, Angew. Chem. 132 (2020) 11898–11905. https://doi.org/10.1002/ange.202002132.
- [15] D.-J. Yoo, J.W. Choi, Elucidating the extraordinary rate and cycling performance of phenanthrenequinone in aluminum-complex-ion batteries, J. Phys. Chem. Lett. 11 (2020) 2384–2392, https://doi.org/10.1021/acs.jpclett.0c00324.
- [16] L.W. Gordon, A.L. Jadhav, M. Miroshnikov, T. Schoetz, G. John, R.J. Messinger, Molecular-scale elucidation of ionic charge storage mechanisms in rechargeable aluminum-quinone batteries, J. Phys. Chem. C 126 (2022) 14082–14093, https://doi.org/10.1021/acs.jpcc.2c04272.
- [17] L.W. Gordon, J. Wang, R.J. Messinger, Revealing impacts of electrolyte speciation on ionic charge storage in aluminum-quinone batteries by NMR spectroscopy, J. Magn. Reson. 348 (2023) 107374, https://doi.org/10.1016/j.jmr.2023.107374.

- [18] D.J. Kim, D.-J. Yoo, M.T. Otley, A. Prokofjevs, C. Pezzato, M. Owczarek, S.J. Lee, J. W. Choi, J.F. Stoddart, Rechargeable aluminium organic batteries, Nat. Energy 4 (2018) 51–59, https://doi.org/10.1038/s41560-018-0291-0.
- [19] L. Zhou, Z. Zhang, L. Cui, F. Xiong, Q. An, Z. Zhou, X.-F. Yu, P.K. Chu, K. Zhang, High-capacity and small-polarization aluminum organic batteries based on sustainable quinone-based cathodes with Al3+ insertion, Cell Rep. Phys. Sci. 2 (2021) 100354, https://doi.org/10.1016/j.xcrp.2021.100354.
- [20] D.-J. Yoo, M. Heeney, F. Glöcklhofer, J.W. Choi, Tetradiketone macrocycle for divalent aluminium ion batteries, Nat. Commun. 12 (2021) 2386, https://doi.org/ 10.1038/s41467-021-22633-y.
- [21] B. Häupler, A. Wild, U.S. Schubert, Carbonyls: powerful organic materials for secondary batteries, Adv. Energy Mater. 5 (2015) 1402034, https://doi.org/ 10.1002/aenm.201402034.
- [22] Y.-T. Kao, S.B. Patil, C.-Y. An, S.-K. Huang, J.-C. Lin, T.-S. Lee, Y.-C. Lee, H.-L. Chou, C.-W. Chen, Y.J. Chang, Y.-H. Lai, D.-Y. Wang, A quinone-based electrode for high-performance rechargeable aluminum-ion batteries with a low-cost AlCl₃ /urea ionic liquid electrolyte, ACS Appl. Mater. Interfaces 12 (2020) 25853–25860, https://doi.org/10.1021/acsami.0c04640.

- [23] J. Revenga, F. Rodríguez, J. Tijero, Study of the redox behavior of anthraquinone in aqueous medium, J. Electrochem. Soc. 141 (1994) 330–333, https://doi.org/ 10.1149/1.2054725.
- [24] L. Yan, C. Zhao, Y. Sha, Z. Li, T. Liu, M. Ling, S. Zhou, C. Liang, Electrochemical redox behavior of organic quinone compounds in aqueous metal ion electrolytes, Nano Energy 73 (2020) 104766, https://doi.org/10.1016/j.nanoen.2020.104766.
- [25] J.D.D.M.E. Poever, The influence of ion association on the polarography of quinone in dimethylformamamide, (1963).
- [26] T. Schoetz, L.W. Gordon, S. Ivanov, A. Bund, D. Mandler, R.J. Messinger, Disentangling faradaic, pseudocapacitive, and capacitive charge storage: A tutorial for the characterization of batteries, supercapacitors, and hybrid systems, Electrochimica Acta 412 (2022) 147002.
- [27] S. Voskian, T.A. Hatton, Faradaic electro-swing reactive adsorption for CO₂ capture, Energy Environ. Sci. 12 (2019) 3530–3547, https://doi.org/10.1039/C9FF02412C.
- [28] K. Deuchert, S. Hünig, Multistage organic redox systems—a general structural principle, Angew. Chem. Int. Ed. Engl. 17 (1978) 875–886, https://doi.org/ 10.1002/anie.197808753.